Analysis and Calibration of the VLP-16 LiDAR for Automotive Applications

Daniela E. Sánchez, *ISTA*
Prof. Thomas Pany, ISTA

BIOGRAPHY (IES)

Daniela E. Sánchez studied Telematics Engineering at Instituto Tecnológico Autónomo de México (ITAM) in Mexico City. She also holds a Master's degree in satellite applications engineering from the Technical University Munich (TUM). She has been a research associate at the Institute of Space Technology and Space Applications (ISTA) since 2017. Her main research area is sensor fusion. Her current research focuses on LiDAR, sensor fusion between LiDAR and GNSS/INS, and relative and absolute navigation algorithms particularly for terrestrial applications.

Prof. Thomas Pany is with the Universität der Bundeswehr München at the faculty of aerospace engineering where he teaches satellite navigation. His research includes all aspects of navigation ranging from deep space navigation to new algorithms and assembly code optimization. Currently he focuses on GNSS signal processing for Galileo second generation, GNSS receiver design, and GNSS/INS/LiDAR/camera fusion. To support this activities, he is developing a modular GNSS test bed for advanced navigation research. Previously he worked for IFEN GmbH and IGASPIN GmbH and is the architect of the ipexSR and SX3 software receiver. He has around 200 publications including patents and one monography.

ABSTRACT

This paper presents advances based on previous studies regarding the analysis and calibration of the 3D LiDAR VLP-16. For this purpose, measurements with the sensor are conducted in facilities particularly dedicated to the calibration of sensors at the University of the German Federal Armed Forces (UniBwM). As it is well known, many terrestrial laser scanner applications, and specifically precise localization for autonomous driving using LiDAR, demand accurate and precise measurements. For this reason, it is of our interest to continue the work of other researching groups (e.g. [1–5]) to characterize errors observed in the measurements of the LiDAR VLP-16. The present study shows the methodology we used to evaluate the performance of each laser channel and characterize them independently of each other. Furthermore, we evaluate the measurements of the sensor in a wide span of ranges, namely from 1 m to 20 m. The results show that a correction can be applied to enhance the accuracy of the range values measured by the sensor.

INTRODUCTION

Light Detection and Ranging (LiDAR) has been used for a wide variety of applications like forestry, structural monitoring and deformation analysis, mobile mapping, autonomous navigation (UAVs, robots, cars, etc.), among others. Particularly for autonomous driving, this technology has emerged as one of the most used due its robustness to scene illumination changes compared to the traditional vision sensors. Contrary to passive sensors, like cameras, LiDAR rely on the backscattering of its own light source. LiDAR is able to provide elevation and azimuth angles, intensity and direct range measurements without the need of any preprocessing step.

In addition, the newest Time Of Flight (ToF) LiDAR models are available in a more compact size and have lower power needs, making them a well-stablished device in the suit of sensors that an autonomous car has. Examples of well-known companies that are working specifically with the Velodyne VLP-16 are Ford, Visteon, Uber, Voyage, Hyundai, Lyft [6–9]. However, it is a mechanical instrument and it is well known that systematic errors can be found due to an imperfection during the manufacturing and assembly of the sensor. For the purposes of our research, which is precise positioning through sensor fusion for autonomous driving, it is a requirement the characterization of the sensors, including the error models. Therefore, it is important to analyze and calibrate the LiDAR that is being used, so those errors can be accounted.

The LiDAR used in the present work is a Velodyne VLP-16, it consists of 16 laser channels that can spin 360 degrees at a rate of 5Hz to 20 Hz, and provides 3D data of the surrounding environment. Due to the number of channels and the vertical Field Of View (FOV), the vertical angular resolution is 2 degrees; while the horizontal resolution, depending at which rate the lasers spin, can vary from 0.1 degrees to 0.4 degrees. The maximum range that the sensor can reach is 100 meters. A summary of the technical specifications can be seen in Table 1.

Table 1. Manufacturer Specifications for the VLP-16 Puck

Sensor	16 lasers
	FOV-V: 30° (+15° to -15°)
	FOV-H: 360 °
	3 cm accuracy
	Time Of Flight (ToF) measurement
Laser	Class 1
	903 nm wavelength
	3.0 mrad horizontal beam divergence
	1.5 mrad vertical beam divergence

Previous studies have already proposed different methods to calibrate other sensors of the same multi-laser scanning line that are manufactured by Velodyne LiDAR. In [1], an extended analysis of the VLP-16 was performed to demonstrate the stability of the measurements during long-term recordings as well as the effect of temperature variations. In their work, it was concluded that it does not appear to be a significant correlation between the temperature and the range bias nor the range noise. However, it is recommended to wait for about 30 minutes to achieve a steady state operating temperature as other Velodyne scanners have shown variations during warm-up time [10].

Even though, the previous analysis demonstrates that the sensor fulfills the manufacturer's stated accuracy in its specifications, the conditions of the study were ideal, i.e. observations were collected at short ranges from the target. Moreover, it highlights as well that some laser channels behave significantly poorer than others. Therefore, the present work shows the methodology we used to evaluate the performance of each laser channel and characterize them independently of each other. Furthermore, we evaluate the measurements of the sensor in a wider range span.

According to [2], the parameters that can be modelled for each laser are:

1. Vertical rotation correction, δ, which is the vertical angular offset of the laser from the scanner's XY plane. In other words, the difference between the laser elevation angle reported by the manufacturer, ω, and the actual angle in which the laser is set, ω_l (See Figure 1[left]).
2. Horizontal rotation correction,β, is the horizontal angular offset of the laser from the zero degree encoder angle, α_ε, about the Z-axis (see Figure 1[right]).
3. Vertical offset, V, is the offset of the laser measurement origin orthogonal to the XY-plane.
4. Horizontal offset, H, is the offset of the laser measurement origin from the Z-axis in the XY plane.
5. Distance offset, D, is an additive constant.
6. Distance scale factor, s.

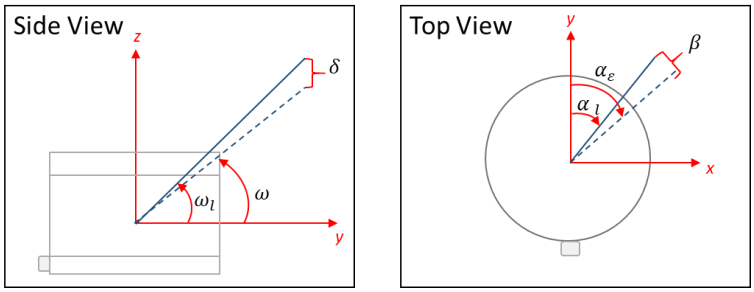

Figure 1. Vertical [left] and horizontal [right] rotation correction for a particular laser

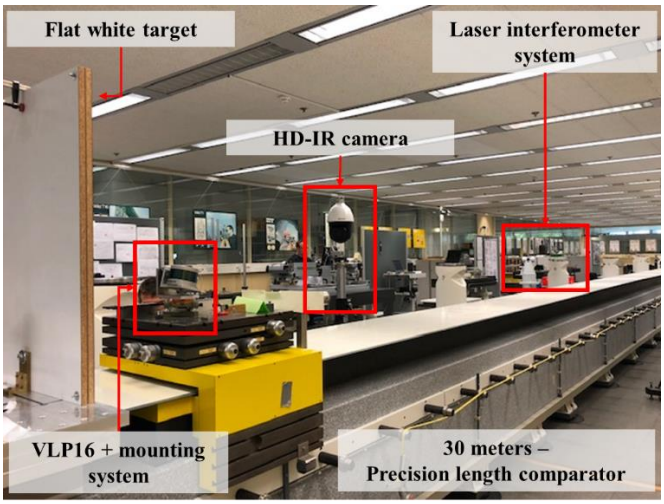

Figure 2. Calibration setup and auxiliary instruments at the laboratory of the Institute of Geodesy (UniBwM)

Mainly, the parameter that we will be focused is the range bias, $\Delta\rho$, which depends on the distance offset, D; a scale factor, s; and a vertical correction according to [11] and is computed as follows:

$$\Delta\rho = D + s\rho + V \sin w_l, \qquad \text{Eq. (1)}$$

where,

ρ is the raw range measurement.

In the following sections we describe: the calibration setup, how it was done the data collection, the geometrical model, the data processing and the results followed by the conclusions.

EXPERIMENTAL DESCRIPTION

Calibration setup

In Figure 2 illustrates the facilities in which we performed the calibration procedure. As seen in the image, a white plane board of approximately 50 cm by 90 cm is used as a target and is fixed at the beginning of a vertical length comparator of 30 m. The vertical comparator has a platform that can be moved along the device with the help of a laser interferometer HP5507B (see Figure 3 [Right]). This platform is used to accurately move the VLP-16 and fix it at different distances along its y-axes from a flat white target. The interferometer has an automatic line capture with an uncertainty of 0.6 µm in its measurements.

The VLP-16 has a special mounting system so that it can be placed on the platform and be leveled correctly (see Figure 4). Additionally, it was designed to steer electronically the laser channels of the sensor and thus, have complete control of the direction in which each of the lasers intersects the surface of the target. This is done by applying a rotation around the x-axis of the sensor using the above mentioned mounting platform. The maximum accuracy of the applied rotation is 1/20 of a degree.

The last element that is shown in Figure 2 is the High Definition Infrared Camera, in order to visualize the lasers on the surface of the target and apply the correct rotation to align the laser to the XY-reference plane of the sensor. The reference is measured with the laser interferometer system and drawn in the surface of the target. This allows us to do two sets of measurements. The first, will allow us to compare the rotation applied through the HD-IR camera and the one that the laser is supposed to have according with the manufacturer's specifications. The second, it gives us a straight forward method to compare the range given by the sensor and the ground truth stablished by the laser interferometer system.

Figure 3. [Left] HD-IR camera. [Right] Laser interferometer

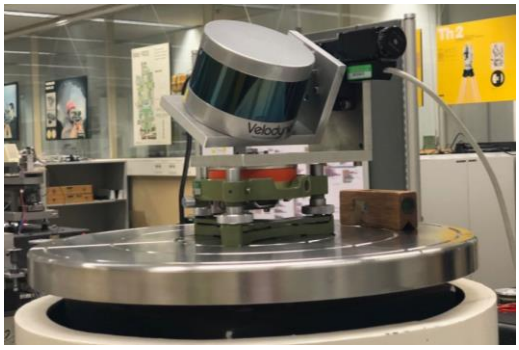

Figure 4. VLP-16 and mounting system

Data collection

Table 2 shows the configuration applied to the sensor for the data collection. It also has to be mentioned that before doing the measurements the sensor had a period of 30 minutes for warming up to get into a steady-state and that it was not powered off until all data collection was finished. For the following two sets of measurements, the VLP-16 was moved along the comparator at a certain distance and measurements were then taken for each laser. That means that 16 point clouds per distance were acquired. The recording of each point cloud had a duration of approximately 20 seconds. Every time that the sensor was moved to the next distance w.r.t. the target, the sensor was leveled to assure it was at 0° degree elevation angle.

Table 2. Configuration used during data collection

Rotation rate	10 Hz
Return mode	Strongest
Phase Lock	off

1. Vertical rotation correction:

For the first part of the calibration, measurements for each laser are taken at 0.75 m, 1m and 2m. Through the mounting system of the VLP-16 the lasers are steered to find the best rotation to be applied, such as the laser is aligned to the XY-reference plane of the VLP-16. As it can be seen in the laser spot pattern in Figure 5, the sensor works with stacked of laser diodes. Each triad comes from a particular laser from the 16 that are integrated in the sensor. The middle laser was taken as a reference for the alignment.

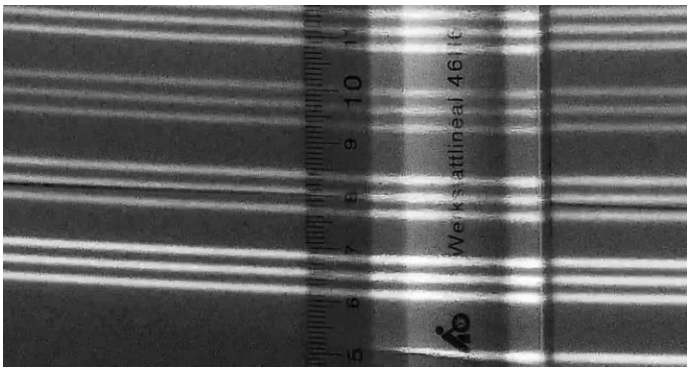

Figure 5. Laser spot pattern on target's surface (image taken from the HD-IR camera)

It is known from the technical specifications that the 16 lasers are individually aimed in 2° increments over the 30° FOV (-15° to + °15). In Table 3, it is shown the values obtained for all channels, where the first half of the channels are those looking upward and the second half downwards.

For the following set of measurements, related with the computation of the distance offset, the angles obtained at 2m are used to align the lasers. It is more distinguishable to align the laser beam spot on the target and assure it is crossing the reference line drawn in the surface, when the beam spot is bigger. The longest distance that the HD-IR camera allowed to visualize the beam spot is at 2 m, therefore we took those angles as reference for the following steps.

One can notice a certain symmetry of the angle in which the lasers are fixed according with the measurements collected at 2m, except for the channels 5 and 12. The angular separation between the lasers is quite close to 2°, being the following pair of channels the ones that have a higher difference (of 0.1°): 4-5, 5-6, 6-7, 7-8 and 15-16.

Table 3. Elevation angle obtained for each laser channel at different distances from the target

Channel	Theoretical El [deg]	El @ 0.75m [deg]	El @ 1m [deg]	El @ 2m [deg]	Hz resolution [deg]	Symmetricity
1	15	14.71	14.35	**14.70**		
2	13	12.30	12.45	**12.75**	1.95	
3	11	10.40	10.55	**10.80**	1.95	
4	9	8.50	8.65	**8.85**	1.95	
5	7	6.40	6.55	**6.75**	2.10	
6	5	4.50	4.65	**4.85**	1.90	
7	3	2.80	2.85	**2.95**	1.90	
8	1	0.80	0.85	**0.95**	2.00	
9	-1	-1.00	-1.05	**-1.00**	1.95	
10	-3	-2.90	-2.95	**-2.95**	1.95	
11	-5	-4.90	-4.95	**-4.95**	2.00	
12	-7	-6.70	-6.80	**-6.90**	1.95	
13	-9	-8.55	-8.75	**-8.85**	1.95	
14	-11	-10.45	-10.65	**-10.80**	1.95	
15	-13	-12.45	-12.65	**-12.80**	2.00	
16	-15	-14.25	-14.45	**-14.70**	1.90	

>= 0.1 deg < 0.1 deg same value

2. Distance offset

After getting the angles in which the lasers can be aligned with the XY-reference plane, the platform of the VLP-16 was positioned to the first distance. For the second set of measurements the sensor was moved to the following distances: 1m, 2m, 4m, 6m , 8m, 10m, 12.5m, 15m, 17.5m and 20m, and in each, a recording using the new rotation angles was performed for each laser.

Another remark to be made is that all physical offsets between the target and the sensor like: offset to the reference point of the moving platform, the location of the mounting system in the platform (as well as height), the mounting point of the VLP-16, the optical center of the sensor were pre-calculated using the interferometer to assure that the distance between the sensor's origin and the board were as expected.

GEOMETRICAL MODEL

In order to compare the measurements done at the laboratory, a geometrical model of the experiment was elaborated, having as input values:

1. The distance to the target, d_t,
2. The rotation applied to the sensor over its X-axis, $R(\omega)$,
3. The sensor properties like the vertical and horizontal resolution (according to the configuration used in the data collection),
4. The target dimensions.

Given a laser spinning over its Z-axis, the intersection of the beam on a planar surface draws a hyperbolic curve on the target, as long as the surface is perpendicular to the XY-plane of the laser and the elevation angle of the laser is different from zero. With that principle the model is constructed, as it can be seen in the blue plot of Figure 6.

A rotation can be applied to the simulated measured data of the target in order to re-compute the data points coordinates:

$$\begin{bmatrix} x' \\ y' \\ z' \end{bmatrix} = R(-\omega_l) \begin{bmatrix} x \\ y \\ z \end{bmatrix}, \quad \text{Eq. (2)}$$

where ω_l is the measured elevation angle for a specific laser channel, as shown in Table 3. The range values can be obtained by

$$\rho = \frac{d_t}{\cos\omega_l \sin\omega \sin\alpha_\varepsilon - \sin\omega_l \cos\omega}, \quad \text{Eq. (3)}$$

The choice of ω_t and d_t depends on the scenario and on the laser channel that is being analyzed.

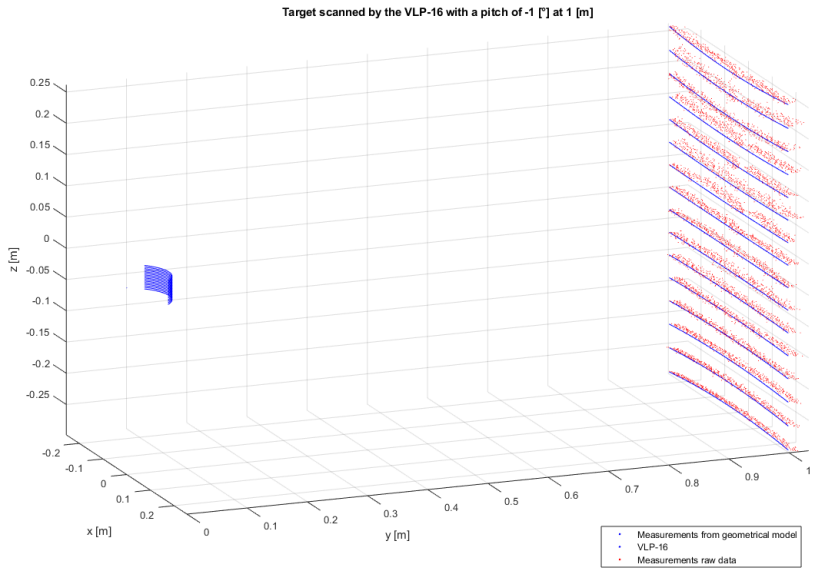

Figure 6. Geometrical model of the calibration setup in blue and raw measurement data in red.

DATA PROCESSING AND CALIBRATION RESULTS

Each of the 160 point clouds obtained and described in the section **Data collection** where pre-filtered in order to remain with the data points belonging to the planar surface. As it was mentioned above, the recordings lasted about 20 seconds, which can be translated to approximately 200 frames per measurement. One can see in Figure 7 the superposed plots from the raw data and the theoretical curve from the geometrical model. The residuals between both are computed and modeled as a normal distribution, from which mean and standard deviation are related to the bias of the measurements and its noise level. The comparison can take different number of frames to evaluate the results. In the present work, all frames were taken into account.

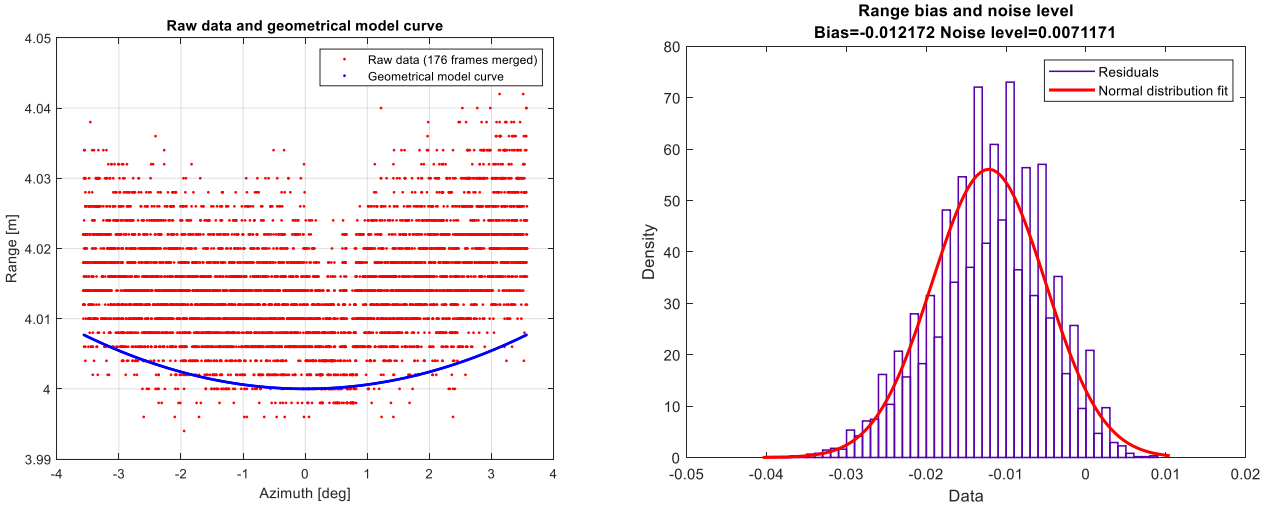

Figure 7. Plot of the geometrical model curve and raw data measurements for a specific laser channel [left]. Distribution of the residuals showing its mean and standard deviation [Right]. Both plots belong to the following scenario: Laser channel 6, where the sensor is at 4m from the target and the rotation applied to the sensor was -4.85°.

For each channel the same process was performed for all the distances in which measurements were done, allowing us to compute the characteristic curve for each laser. In Figure 8, an example of the range bias and range noise is shown for laser channel 6.

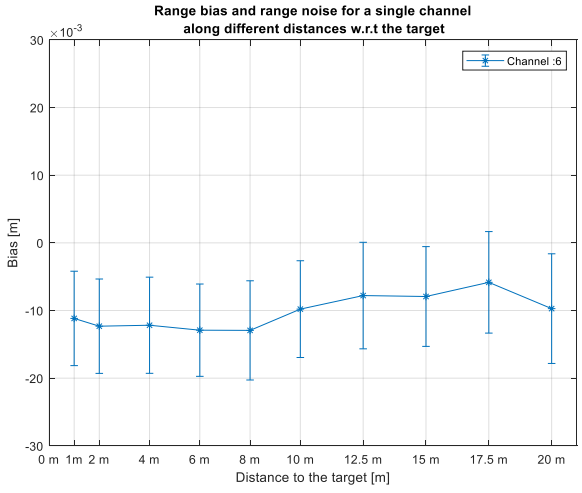

Figure 8. Characteristic curve for laser channel 6

The remaining results are shown in Figure 9 and Figure 10. Figure 9 shows the characteristic curves for lasers that have an elevation angle above 0°, and Figure 10, the ones that are looking downwards.

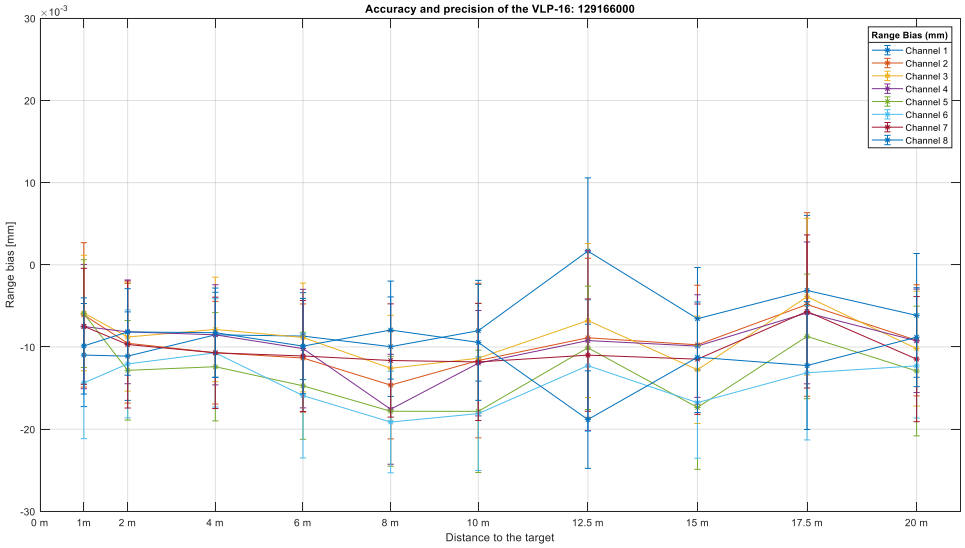

Figure 9. Characteristic curve for the first eight laser channels (Elevation angles above 0°)

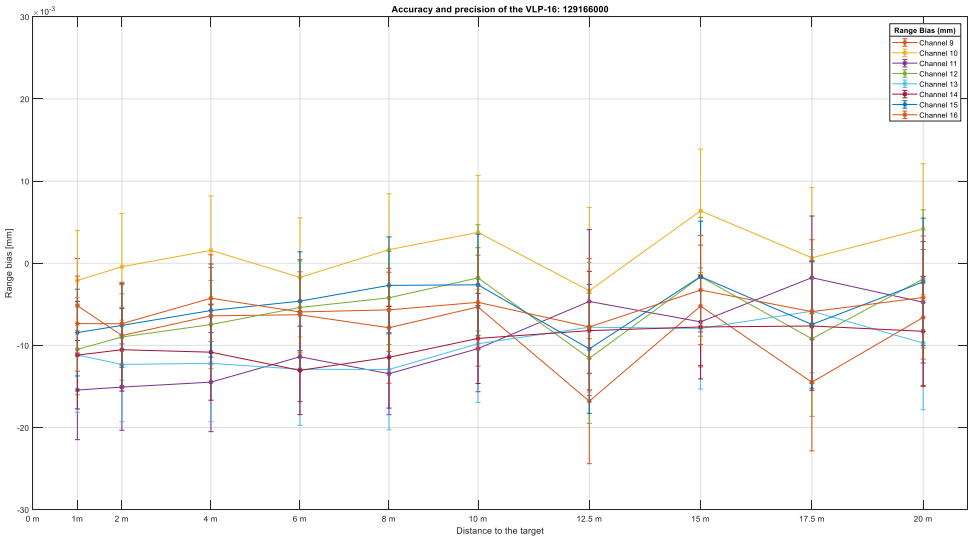

Figure 10. Characteristic curve for the last eight laser channels (Elevation angles below 0°)

CONCLUSIONS AND REMARKS

This paper shows the procedure we followed for the calibration of the VLP-16. Our purpose is to inquire the individual behavior of each of the 16 lasers that compose the sensor. With the help of auxiliary tools of high precision we are able to perform a direct method for the comparison of the range values that should be obtained by the sensor. As it has been shown, the sensor complies with the accuracy specification of +/- 3 cm, given by the manufacturer. Contrary to [1], the analysis does not show a particular low performance in the most downward looking lasers, namely 14, 15 and 16, according with our numeration (see Table 3). In Figure 11, the particular curves obtained for those laser channels can be seen. In general, we observed stable measurements which start slightly to bounce after 10 m, even though this behavior was expected to appear at very short distances to the target. At short distances, the sensor may be pushed to a saturation mode or the laser pulse may not have enough

time of flight to compute the range measurements. This study agrees with [1] for a wider span of distances, the maximum range bias found is 20 mm, and the range noise vary from 4.9 mm to 11.2 mm. Table 4 shows a summarized version of the results shown in previous figures, where it illustrates the overall performance of each laser.

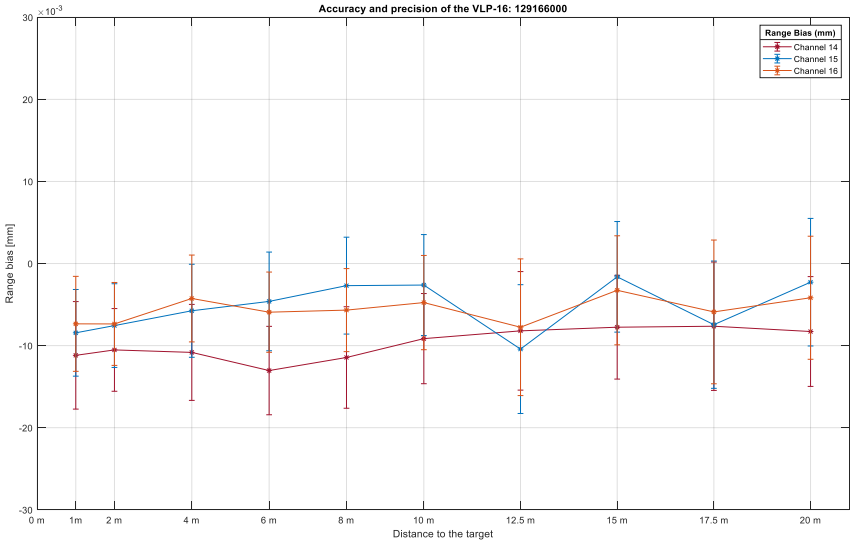

Figure 11. Characteristic curves for the last three channels (facing downwards)

As our main focus in our research is directed to precise localization for autonomous driving, we do not consider that corrections using the obtained bias will impact significantly later steps in our processing. However, it is of great significance to know what to expect from the sensor, especially with measurements collected at farther distances from the target.

Future work may be focused in the analysis of the intensity data given by the sensor, as it is of our interest to exploit this source of information. From some of the recordings done at the beginning of our measurements, we saw the impact on the range values of a metallic object which was lying in the surface of the target. An example of this jump can be seen in Figure 12.

Table 4. Minimum and maximum range bias and noise bias for the 16 laser channels that compose the VLP-16

Channel	Range bias [min, max] [m]	Range noise [min, max] [m]	No. of frames considered in avg.
1	[0.0017 ,0.0111]	[0.0052 , 0.0091]	192.0
2	[0.0048 ,0.0146]	[0.0062 , 0.0112]	187.4
3	[0.0039 ,0.0128]	[0.0064 , 0.0095]	188.4
4	[0.0058 ,0.0176]	[0.0061 , 0.0109]	188.4
5	[0.0059 ,0.0178]	[0.0061 , 0.0079]	188.1
6	[0.0107 ,0.0191]	[0.0062 , 0.0082]	188.1
7	[0.0057 ,0.0118]	[0.0067 , 0.0093]	188.1
8	[0.0079 ,0.0188]	[0.0053 , 0.0078]	187.4
9	[0.0052 ,0.0168]	[0.0057 , 0.0084]	189.7
10	[0.0004 ,0.0064]	[0.0061 , 0.0101]	189.7
11	[0.0018 ,0.0154]	[0.0050 , 0.0087]	187.4
12	[0.0016 ,0.0116]	[0.0053 , 0.0094]	187.4
13	[0.0058 ,0.0129]	[0.0068 , 0.0081]	187.4
14	[0.0076 ,0.0130]	[0.0050 , 0.0078]	186.1
15	[0.0016 ,0.0104]	[0.0051 , 0.0078]	187.4
16	[0.0033 ,0.0078]	[0.0049 , 0.0088]	187.4

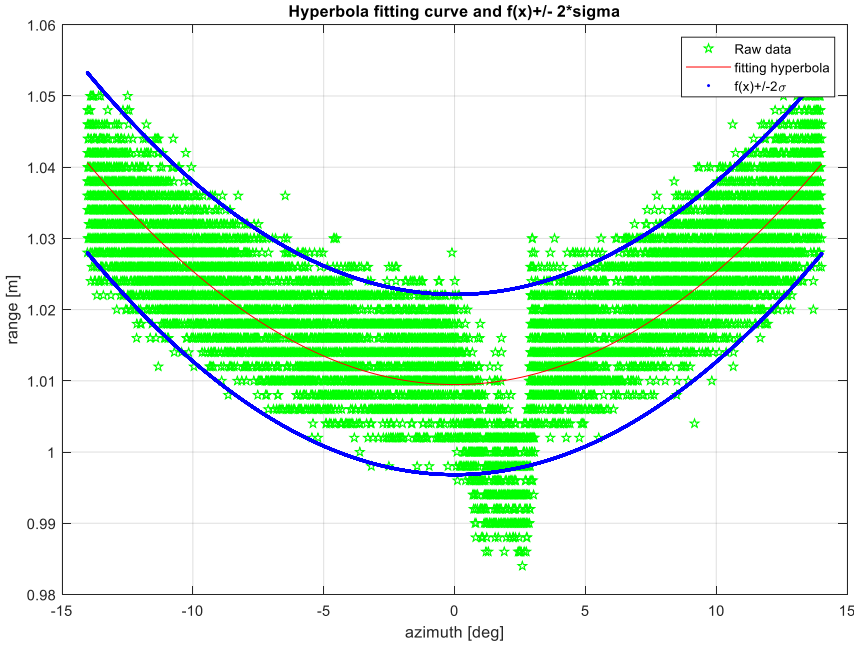

Figure 12. Example of how saturation may induce errors in the range computation, either by shortening or lengthened them.

ACKNOWLEDGMENTS

Special acknowledgment to Dipl.-Ing. Wolfgang Liebl, head of laboratory, and Günter Kraus, precision mechanical technician at the Institute of Geodesy in UniBw München for providing access and use of the facilities as well as their support for the construction of the VLP-16 mounting system. M. Sc. Andreas Schütz is also thanked for his assistance during the data collection, as well as Tikkanien Severi Adrian. The results presented in this work were developed within the project "OPtimal Assistierte, hoch Automatisierte, Autonome und cooperative Fahrzeugnavigation und Lokalisation (short: OPA3L)", funded by the German Federal Ministry for Economic Affairs and Energy (BMWi) and administered by the Project Management Agency for Aeronautics Research of the German Space Agency (DLR) in Bonn, Germany (grant no. 50NA1910). Any opinions, findings, conclusions, or recommendations expressed in this material are those of the author and do not necessarily reflect the views of UniBwM nor DLR.

REFERENCES

[1] C. L. Glennie, A. Kusari, and A. Facchin, "CALIBRATION AND STABILITY ANALYSIS OF THE VLP-16 LASER SCANNER," *Int. Arch. Photogramm. Remote Sens. Spatial Inf. Sci.*, vol. XL-3/W4, pp. 55–60, 2016.

[2] C. Glennie and D. D. Lichti, "Static calibration and analysis of the Velodyne HDL-64E S2 for high accuracy mobile scanning," *Remote Sensing*, vol. 2, no. 6, pp. 1610–1624, 2010.

[3] D. D. Lichti and M. G. Licht, "Experiences with terrestrial laser scanner modelling and accuracy assessment," *Int. Arch. Photogramm. Remote Sens. Spat. Inf. Sci*, vol. 36, no. 5, pp. 155–160, 2006.

[4] F. M. Mirzaei, D. G. Kottas, and S. I. Roumeliotis, "3D LIDAR–camera intrinsic and extrinsic calibration: Identifiability and analytical least-squares-based initialization," *The International Journal of Robotics Research*, vol. 31, no. 4, pp. 452–467, 2012.

[5] D. Schneider, "Calibration of a Riegl LMS-Z420i based on a multi-station adjustment and a geometric model with additional parameters," *Int. Arch. Photogramm. Remote Sens. Spat. Inf*, vol. 38, pp. 177–182, 2009.

[6] *visteon-participates-research-project-validating-autonomous.* [Online] Available: https://www.visteon.com/newsroom/visteon-participates-research-project-validating-autonomous-driving-systems/. Accessed on: Sep. 26 2019.

[7] *Peter Rander, President, Author at Argo AI.* [Online] Available: https://www.argo.ai/author/peter-rander/. Accessed on: Sep. 26 2019.

[8] *Yandex Self-Driving Cars.* [Online] Available: https://sdc.yandex.com/. Accessed on: Sep. 26 2019.

[9] O. Cameron, *Introducing the Voyage G2 Autonomous Vehicle.* [Online] Available: https://news.voyage.auto/introducing-the-voyage-g2-autonomous-vehicle-5e15cca399b5. Accessed on: Sep. 26 2019.
[10] C. Glennie and D. D. Lichti, "Temporal stability of the Velodyne HDL-64E S2 scanner for high accuracy scanning applications," *Remote Sensing*, vol. 3, no. 3, pp. 539–553, 2011.
[11] G. Vosselman and H.-G. Maas, *Airborne and terrestrial laser scanning*: CRC Press, 2010.